

## Systematic Studies of the Square-Hexagonal Flux Line Lattice Transition in $\text{Lu}(\text{Ni}_{1-x}\text{Co}_x)_2\text{B}_2\text{C}$ : The Role of Nonlocality

P. L. Gammel and D. J. Bishop

*Bell Laboratories, Lucent Technologies, Murray Hill, New Jersey 07974*

M. R. Eskildsen, K. Mortensen, and N. H. Anderssen

*Risø National Laboratory, DK-4000 Roskilde, Denmark*

I. R. Fisher, K. O. Cheon, P. C. Canfield, and V. G. Kogan

*Ames Laboratory and Department of Physics and Astronomy, Iowa State University, Ames, Iowa 50011*

(Received 25 September 1998)

We have studied, using small angle neutron scattering, the flux line lattice square to hexagonal symmetry transition in single crystal  $\text{Lu}(\text{Ni}_{1-x}\text{Co}_x)_2\text{B}_2\text{C}$ . Low Co concentrations ( $x < 0.1$ ), which reduce the mean free path and increase the coherence length, also move the structural transition to higher fields than in the undoped system. These data, quantitatively understood within the framework of a theory that includes nonlocal corrections to the London model due to the Fermi surface anisotropy, can be modeled using a simple ratio of the nonlocality range to the intervortex spacing. [S0031-9007(99)09186-3]

PACS numbers: 74.60.Ge, 74.60.Ec, 74.62.Dh

Studies of the vortex lattice in the rare-earth (RE) nickel-borocarbide magnetic superconductors have uncovered many interesting and novel results. This class of superconductors with the generic formula  $(\text{RE})\text{Ni}_2\text{B}_2\text{C}$  where RE = Y, Lu, Tm, Er, Ho, and Dy comprises materials with moderately high  $T_c$  and both antiferromagnetic and nonmagnetic members [1]. New flux line lattice (FLL) physics seen in studies of these compounds includes a square vortex lattice [2], a field-driven square to hexagonal symmetry transition [3], a static disordering at high fields [4], a coupling between the underlying spin-density wave order and the FLL structure [5], and a field-driven rotation of the low field, rhombic FLL [6].

The field-driven structural transitions are a particularly interesting example of new vortex physics in this system. Qualitatively, they can be understood as being due to the anisotropy of the Fermi surface in these compounds, which gives rise to a slight fourfold modulation of the current distribution associated with the flux lines. At low magnetic fields, when the vortices are far apart, this anisotropy matters little and one finds hexagonal vortex lattices as would be expected for cylindrical vortex lines, with an isotropic current and field distribution. At these low fields, there is still an effect of the Fermi surface anisotropy, which breaks the orientational degeneracy, locking the FLL relative to the crystallographic directions. As the field is increased, there is a transition where this orientational ordering rotates by  $45^\circ$  [6]. At still higher fields, when the vortices are closer together, the anisotropy becomes more important and drives a transition from the low field hexagonal phase to the high field, square phase [3]. Both transitions were previously observed, but only qualitative comparison to the detailed theory incorporat-

ing nonlocal corrections to the London model and Fermi surface anisotropy [7] could be made. This theory also predicts that the square-hexagonal transition should depend strongly on the electronic mean free path  $\ell$  and the superconducting coherence length  $\xi$  of the sample. Intuitively, one can see that the shorter  $\ell$  is, the more isotropic the materials are, and the higher in field one will need to go to drive the hexagonal to square transition. This paper is a report on the first quantitative experimental test of this theory using these dependencies.

The system we have chosen to study is single crystal  $\text{Lu}(\text{Ni}_{1-x}\text{Co}_x)_2\text{B}_2\text{C}$ , with Co dopings  $x < 0.09$ . Previous studies [8] have shown that Co substitution on the Ni site is a nonmagnetic impurity that suppresses  $T_c$  by reducing the density of states  $N(0)$  at the Fermi level. This system is an ideal choice for our studies for a variety of reasons: The parent compound is nonmagnetic, large single crystals can be grown, the penetration depth is sufficiently short so that the neutron reflectivity from the FLL is large, which results in good signal-to-noise small-angle neutron scattering (SANS) data and, finally, all compounds have a high  $T_c$ , simplifying the cryogenics. For the parent compound with  $x = 0$ ,  $T_c = 16.0$  K,  $H_{c2} \sim 90$  kOe,  $\ell \sim 27$  nm, and  $\rho_0 \sim 1.5 \mu\Omega$  cm, where  $\rho_0$  is the residual resistivity. For compounds with  $x < 0.1$ ,  $T_c$  and  $\rho_0$  are found to scale roughly linearly with doping [8]. For the highest doping reported here,  $x = 0.09$ ,  $T_c = 9.5$  K,  $H_{c2} = 22$  kOe,  $\ell \sim 3$  nm, and  $\rho_0 \sim 14.5 \mu\Omega$  cm.

To avoid well-known difficulties with polycrystalline samples, only high quality single crystals were used for this study. They were grown from a  $(\text{Ni}_{1-x}\text{Co}_x)_2\text{B}$  flux, similar to other  $(\text{RE})\text{Ni}_2\text{B}_2\text{C}$  single crystals and described elsewhere [9]. Particular care was taken to have the same

cobalt concentration in both the flux and the polycrystalline starting material. The samples used here were platelets with typical areas of 18–70 mm<sup>2</sup> exposed to the neutron beam, thickness between 0.5–0.7 mm, and masses of 141–539 mg. The range of parameters reflects the non-systematic variation in the size of the largest crystals as a function of doping. The *c* axis is always perpendicular to the platelet and for all the experiments described here, the magnetic field was applied parallel to the *c* axis. The data discussed here were taken at 2.0 K after field cooling. The  $T_c$ 's of the large crystals required for SANS studies were found to correlate well with other studies of this system [8], and thus we are confident of the cobalt concentration  $x$ , within  $\pm 0.005$ .

The experiments described here were SANS studies performed at the cold neutron guide hall of the DR3 reactor at Risø National Laboratory. The incident neutrons were applied essentially parallel to both the *c* axis of the crystal and the magnetic field. The neutrons had a wavelength  $\lambda_n$  between 5.4 and 15.3 Å, a wavelength spread  $\Delta\lambda_n/\lambda_n \sim 18\%$ , and angular divergences between 0.095° and  $\sim 0.15^\circ$  FWHM depending on sample size and neutron collimation. An area detector at the end of a 6-m evacuated chamber counted the neutrons, which were Bragg scattered from the magnetic field pattern in the sample due to the FLL. Because of the high quality of the samples, the rocking curve widths tended to be small, typically a few tenths of a degree, and in most cases less than the scattering angle. Since this study focused on the symmetry of the FLL, rather than absolute measurements of the form factor, which determines the integrated intensity of the Bragg peaks, the data were principally taken by summing two-dimensional diffraction patterns with the cryostat at the locations of the first order FLL Bragg peaks.

The rocking curves were also studied as both a function of applied field and doping. Careful studies for  $x = 0.045$  and sparser data at other dopings revealed no changes in the rocking curves for the doped samples. This indicates that the longitudinal correlation lengths [3,4] for the undoped and lightly doped samples were quite similar and that the doping did not disorder the lattice in any measurable way. We conclude from this that the dopants do not act as strong pinning centers for the FLL in this system.

In the pure system, with  $x = 0$ , the onset of the square to hexagonal transition was previously found to occur in the 0.75–1.25 kOe range. What one sees experimentally [3] is that at high fields, one has four sharp, well-defined (1,0) first order FLL Bragg peaks and four weaker (1,1) second order peaks. As the field is reduced and the square-to-hexagonal transition is approached, the four (1,0) peaks each split in the azimuthal direction and move out slightly in reciprocal space position normalized to  $H^{1/2}$ , while the four (1,1) peaks show a reduction in normalized peak position. These combined motions produce the twelve first order FLL Bragg peaks associated with two hexagonal lattices, which are separated in two domains, rotated by 90°.

The change in magnitude of the reciprocal space position is a simple manifestation of the 7% more efficient packing of the hexagonal lattice relative to the square lattice.

Shown in Fig. 1 is an example of our raw data for a doped sample with  $x = 0.045$ , at a temperature of 2.0 K and for two applied fields, 10 kOe and 4 kOe. The main results of this paper are evident in this data. In the 10 kOe data one can see the Bragg scattering pattern from a well-defined square lattice with four sharp first order (1,0) FLL Bragg peaks. In the 4 kOe data, the FLL is well into the transition region as the (1,0) peaks are already split by  $\sim 16^\circ$ . Clearly, in qualitative agreement with the theoretical prediction, a doping of  $x = 0.045$  has moved the transition to significantly above the pure system value.

To make a quantitative comparison with theory, we have looked at the azimuthal distribution of the scattered

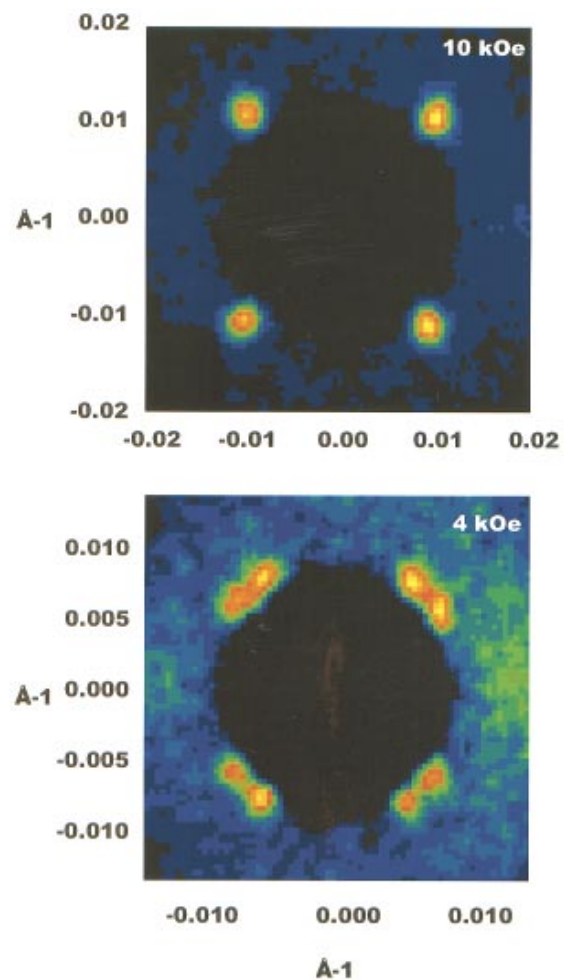


FIG. 1(color). Shown are two FLL diffraction patterns for  $\text{Lu}(\text{Ni}_{0.955}\text{Co}_{0.045})_2\text{B}_2\text{C}$  at  $T = 2.0$  K. In the top panel, at  $H = 10$  kOe, the FLL is square, as is evident from the four bright (1,0) first order FLL Bragg peaks. Weak scattering near  $q = 0$  due to defects in the crystal, unrelated to the FLL, has been subtracted off. As the field is lowered to 4 kOe, the (1,0) peaks begin to split as shown in the lower panel. Fits to the azimuthal intensity distribution give a splitting of  $16^\circ$  for this field.

intensity. At each field, the data were analyzed in reciprocal space as a function of angle for a constant magnitude of the scattering vector,  $q = 2\pi(B/\phi_0)^{1/2}$ . For a square FLL, the azimuthal intensity distribution has four peaks spaced by  $90^\circ$ . As the field is lowered through the transition, each of the four peaks splits, with the magnitude of the splitting eventually going to  $30^\circ$  when the FLL transforms into two hexagonal domains. Observing the onset of continuous symmetry transitions is inherently difficult as the first signature of the splitting is an azimuthal broadening comparable with both the experimental resolution and the intrinsic width due to lattice imperfections. In general, the azimuthal splitting was only directly observable when it was above  $10^\circ$ . However, insight into the details of the onset of the symmetry transformation can be obtained by looking at the azimuthal broadening. To study the nature of the symmetry transition, two different measurement schemes were used. When the split was clearly resolved, the measurements were performed at constant neutron wavelength. When the split could not be resolved, measurements of the azimuthal width were performed in order to keep the experimental resolution functions constant. This was done by changing the wavelength and the applied field in concert to keep the scattering angle,  $2\theta = q\lambda_n/2\pi$ , constant. In this way the widths at different fields can be compared directly, and the onset of the transition is equivalent to the onset of the azimuthal broadening.

Shown in Fig. 2 are examples of these two types of data for  $x = 0.015, 0.045, 0.06$ , and  $0.09$ . At high fields, the

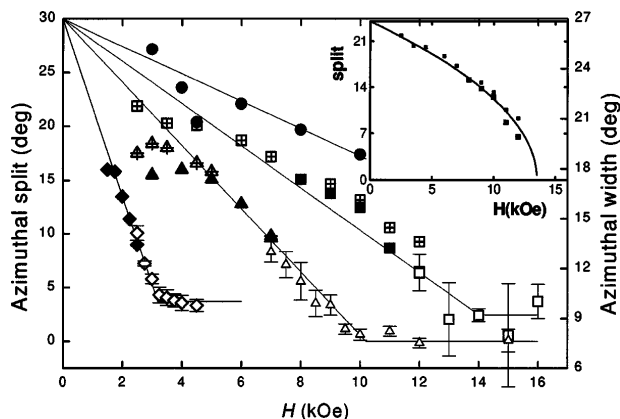


FIG. 2. This plot shows the azimuthal splitting described in Fig. 1 for the different fields and Co dopings of this study. The data are indicated as follows:  $x = 0.015$  by diamonds,  $x = 0.045$  by triangles,  $x = 0.06$  by squares, and  $x = 0.09$  by circles. The two different types of experiment give the different ordinates for splitting (solid and partially filled symbols) and width (open symbols), which have been adjusted to overlap. The lines are linear fits, pinned to agree with the known, isotropic hexagonal lattice at low fields (corresponding to  $30^\circ$  splitting in this notation). Also shown in the inset is a fit to the square root field dependence, predicted to be valid near the transition for  $x = 0.06$  Co doping.

azimuthal width is field independent. At a specific, doping dependent field, it begins to increase. Data derived from this width are shown by the open symbols in Fig. 2, and scaled by the right-hand ordinate. Well below where the transition begins, we are able to resolve the peak splitting instead of just broadening, which data are shown by the filled and centered points in Fig. 2, and scaled by the left hand ordinate. The two ordinates in Fig. 2 are calibrated using the data in the regime of overlap. At very low fields, preliminary decoration experiments have shown the expected undistorted hexagonal lattice.

In examining the data, a number of points become clear. For increased doping, the transition clearly moves to higher fields. Secondly, a linear extrapolation of the split data to the high field asymptote, as shown by the lines in Fig. 2, gives a value of the “transition” which agrees within measurement errors with a value obtained by calling the transition the field where the width just begins to increase. Near the transition, the mean field theory predicts a square root singularity in the splitting,  $\Delta\Theta = \Theta_0[1 - H/H_{\text{trans}}]^{1/2}$ . Shown in the inset to Fig. 2 is an example of such a fit for  $x = 0.06$  using  $\Theta_0 = 24^\circ$  and  $H_{\text{trans}} = 13.5$  kOe, which also is in good agreement with the theory, although both the width of the region over which the fit should work and how to compare the prefactor  $\Theta_0$  to theory are still open questions. Fitting all the data to the square root singularity causes only small ( $<1.5$  kOe) shifts in the definition of the transition field, which do not affect the discussion below. Finally, it is clear that one can move the transition field high enough that one can study the entire region with SANS alone. This is a significant experimental advantage. In the original work where the square to hexagonal transition was first seen [3], the field at which it occurred was at an awkward value, too high for magnetic decoration and too low for SANS. Doping can clearly move the transition to at least  $20\times$  higher in field which will make the entire transition much more accessible to a number of techniques including both SANS and STM [2,10].

The transition field,  $H_{\text{trans}}$ , can be calculated numerically within the London model corrected for nonlocality [7]. Physically, the structural phase transition at  $H_{\text{trans}}$  occurs when the energy associated with nonlocal corrections to the field distribution becomes comparable to the shear energy of the FLL. Qualitatively, the transition happens when the nonlocality range  $\rho(T, \ell)$  becomes a certain fraction of the intervortex spacing  $a_0$ ,  $\rho = Ca_0$ , with  $C$  a constant. Then  $H_{\text{trans}} = \phi_0/a_0^2 = C^2\phi_0/\rho^2$ . Empirically we find  $C = 0.065$ , which is reminiscent of the Lindemann criterion, which states that the FLL melting transition occurs when the thermal vibrations are a fraction of the intervortex spacing [11]. The nonlocality range can be expressed [7] as  $\rho \sim \xi_0[\gamma(T, \ell)/2]^{1/2}$ . In this expression  $\xi_0$  is the BCS, zero temperature coherence length and the temperature and mean-free path dependent factor  $\gamma$  can, in general, be evaluated only numerically. However, at the low reduced temperatures of interest here,

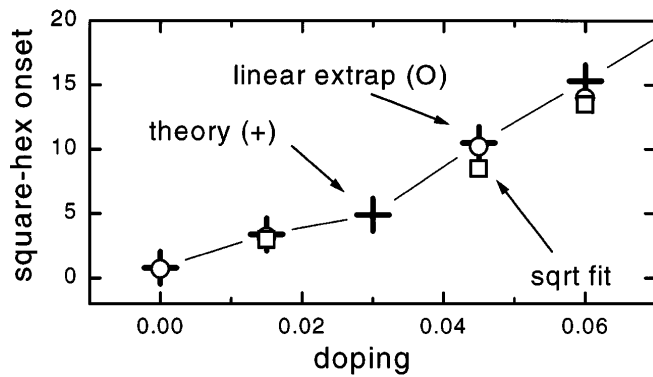


FIG. 3. Shown are the transition fields versus doping using linear extrapolations (○), square root (□) fits, and from theory using the transport data (+).

the zero temperature analytic result for  $\gamma$  is available. Although the exact result is cumbersome, this  $T = 0$  result can be approximated quite accurately by the polynomial  $\gamma(0, \ell)^{-1} = 3[1 + 1.66(\xi_0/\ell) + 0.581(\xi_0/\ell)^2]/2$ , valid for  $\xi_0/\ell < 11$  which covers all dopings except  $x = 0.09$ . This yields  $H_{\text{trans}} = (3\phi_0 C^2/\xi_0^2)[1 + 1.66(\xi_0/\ell) + 0.581(\xi_0/\ell)^2]$ .

Shown in Fig. 3 is a summary of our doping data. Shown by the open symbols are the transition fields, taken from linear (○) and square root (□) fits to the splitting versus field as a function of Co concentration. For comparison, we have also plotted the predictions of the theory outlined above. The values of  $\xi_0/\ell$  were obtained for our samples using the resistivity and transition temperature  $T_c$  for each doping [8]. For our samples we find  $\xi_0/\ell$  is equal to 1.1, 3.3, 7.8, 11, and 17 for  $x = 0, 0.015, 0.045, 0.06$ , and 0.90. More extensive tabulated results are given in [8]. Using the formula for  $H_{\text{trans}}$ , the theoretical points in Fig. 3 were calculated. Clearly, the agreement between data and theory is excellent. Also clear is that we have captured the important range of doping, as the extrapolated square-hexagonal transition field for  $x = 0.09$  already is in the nonphysical regime above  $H_{c2}$ .

In conclusion, we have presented the results of a systematic study of the doping dependence of the square to

hexagonal FLL structural phase transition in crystals of  $\text{Lu}(\text{Ni}_{1-x}\text{Co}_x)_2\text{B}_2\text{C}$ . Our data show that as the doping increases, the mean-free path  $\ell$  decreases and the coherence length  $\xi$  grows, and the transition moves to significantly higher fields. Our results agree quantitatively with the theoretical predictions, although detailed comparison to the square root field dependence near the transition remains an open question. We believe that this new effect, in addition to validating our understanding of the microscopic origins of the square to hexagonal FLL structural phase transition, also gives us an important new tool with which to manipulate the transition and move it into other, more accessible experimental regimes.

- [1] R. J. Cava *et al.*, *Physica (Amsterdam)* **235C**, 154 (1994); P. C. Canfield, P. L. Gammel, and D. J. Bishop, *Phys. Today* **51**, No. 10, 40–46 (1998).
- [2] U. Yaron *et al.*, *Nature (London)* **382**, 236 (1996); M. Yethiraj *et al.*, *Phys. Rev. Lett.* **79**, 4849 (1997); Y. DeWilde *et al.*, *Phys. Rev. Lett.* **78**, 4273 (1997).
- [3] M. R. Eskildsen *et al.*, *Phys. Rev. Lett.* **78**, 1968 (1997).
- [4] M. R. Eskildsen *et al.*, *Phys. Rev. Lett.* **79**, 487 (1997).
- [5] M. R. Eskildsen *et al.*, *Nature (London)* **393**, 242 (1998).
- [6] D. McK. Paul *et al.*, *Phys. Rev. Lett.* **80**, 1517 (1998); V. G. Kogan, P. Miranovic, and D. McK. Paul, in *The Superconducting State in Magnetic Fields: Special Topics and New Trends*, edited by C. A. R. Sa de Melo Directions in Condensed Matter Physics Vol. 13 (World Scientific, Singapore, 1998).
- [7] V. G. Kogan *et al.*, *Phys. Rev. B* **54**, 12386 (1996); V. G. Kogan *et al.*, *Phys. Rev. B* **55**, R8693 (1997); V. G. Kogan *et al.*, *Phys. Rev. Lett.* **79**, 741 (1997).
- [8] K. O. Cheon *et al.*, *Phys. Rev. B* **58**, 6463 (1998); H. Schmidt and H. F. Braun, *Phys. Rev. B* **55**, 8497 (1997).
- [9] B. K. Cho *et al.*, *Phys. Rev. B* **52**, 3684 (1995); M. Xu *et al.*, *Physica (Amsterdam)* **227C**, 321 (1994).
- [10] I. Magio-Aprile *et al.*, *Phys. Rev. Lett.* **75**, 2754 (1995).
- [11] A. Houghton, R. A. Pelcovits, and A. Sudbø, *Phys. Rev. B* **40**, 6763 (1989); M. A. Moore, *Phys. Rev. B* **39**, 136 (1989).